Water Research 266 (2024) 122410

Contents lists available at ScienceDirect

Water Research

journal homepage: www.elsevier.com/locate/watres

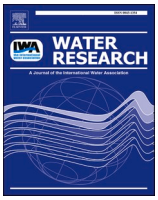

Photoaged tire wear particles hinder the transport of Pb(II) in urban soils under acid rain: Experimental and numerical investigations

Enjie Li [a,b], Jinhui Huang [a,b,*], Hanbo Yu [c,d], Si Liu [a,b], Wenjuan He [a,b], Wei Zhang [a,b], Haoliang Pang [a,b], Chenyu Zhang [a,b]

[a] College of Environmental Science and Engineering, Hunan University, Changsha 410082, PR China
[b] Key Laboratory of Environmental Biology and Pollution Control (Hunan University), Ministry of Education, Changsha 410082, PR China
[c] School of Hydraulic and Environmental Engineering, Changsha University of Science & Technology, Changsha 410114, PR China
[d] Key Laboratory of Dongting Lake Aquatic Eco-Environmental Control and Restoration of Hunan Province, Changsha 410114, PR China

ARTICLE INFO

Keywords:
Tire wear particles
Aging
Lead transport
Acid rain
Urban soil
Environmental risk

ABSTRACT

Rapid urbanization brought lots of serious environmental contamination, including the accumulation of heavy metals, acid rain, and the emission of tire wear particles (TWPs), with detrimental effects for terrestrial ecosystems. Nevertheless, how naturally aged TWPs affect the mobilization of heavy metals in soils under acid rain is still unclear. Here, we investigate the adsorption and transport mechanisms of Pb(II) co-existing with acid rainwater in soil-TWP mixtures via batch experiments, column experiments and modeling. Results showed that photoaged TWP significantly prolonged the Pb(II) adsorption equilibrium time (1 to 16 h) and enhanced the Pb (II) adsorption capacity of soils. Soil column profiles confirmed that TWP effectively boosted the initial accumulation of lead in the topsoil and thus impeded the downward transport of lead. The retardation factor (R) estimated by the linear two-site sorption model (TSM) fitting the Pb(II) breakthrough curves gradually increased from 1.098 to 16.38 in soils with TWP (0–10 %). Comparative results of linear or nonlinear TSM suggested nonlinear sorption replacing linear sorption as the main Pb(II) sorption mechanism under 1 % and 10 % TWP. This research provides significant insights into the implications of TWP on the Pb(II) retention behaviors and highlights the severer potential remobilization risks of Pb(II) in urban soils under different acid rain environments.

1. Introduction

Plastics have brought great convenience to mankind's lives owing to their superior features, such as low cost, portability, and durability (Wen et al., 2024). However, plastic products are fragmented into smaller pieces via physical, chemical, and biological roles in the environments, creating widespread pollution of microplastics (MPs) (He et al., 2023; Luo et al., 2021; Winkler et al., 2019). Tire wear particles (TWPs), primarily generated by the friction between tyres and roads surfaces, as well as through running tracks, artificial turf, and rubber mats via irradiation, mechanical abrasion, and biological breakdown, have been recognized as a main source of MPs. Rapid urbanization in recent decades has led to a worldwide average release amount of 0.81 kg/year per individual of TWPs into the surrounding environments (Kole et al., 2017). Comprehensive calculations show that the majority of TWPs (66–76 %) is deposited into the soil. A smaller proportion (12–20 %) is released into surface water, while only 2–10 % of TWPs is emitted into the atmosphere (Chen et al., 2024). Nevertheless, compared with traditional MPs, the more complex compositions of TWPs, which consist of rubber, vulcanization agents, reinforcing agents, antioxidants, etc. (Castan et al., 2022), may lead to the release of a greater amount of hazardous chemicals (e.g., polychlorinated biphenyl, polycyclic

Abbreviations: TWP, Tire wear particle(s); V-TWP, Virgin tire wear particle; A-TWP, Photoaged tire wear particle; MPs, Microplastics; SAR, Simulated acid rain; Pure Soil, Soil without artificially added tire wear particle; $S + 0.1$ % V-TWP/A-TWP, Soil with artificially added 0.1 % V-TWP/A-TWP; $S + 1$ % V-TWP/A-TWP, Soil with artificially added 1 % V-TWP/A-TWP; $S + 10$ % V-TWP/A-TWP, Soil with artificially added 10 % V-TWP/A-TWP; BTCs, Breakthrough curves; CDM, Convection-dispersion model; TSM, Two-site sorption model; SEM, Scanning electron microscopy; FTIR, Fourier transform infrared spectrometer; TGA, Thermogravimetric analyzer; XPS, X-ray photoelectron spectrometer.

* Corresponding author at: College of Environmental Science and Engineering, Hunan University, Changsha 410082, PR China.
E-mail address: huangjinhui@hnu.edu.cn (J. Huang).

https://doi.org/10.1016/j.watres.2024.122410
Received 16 July 2024; Received in revised form 27 August 2024; Accepted 6 September 2024
Available online 7 September 2024

aromatic hydrocarbons, and heavy metals) into the surrounding environment (Sun et al., 2024; Wagner et al., 2018; Xu et al., 2023). It is proposed that, in addition to leachate, TWPs themselves may cause toxicological impacts on ecosystems (Liu et al., 2022b; McIntyre et al., 2021). Consequently, the European Union has taken the lead in banning MPs, including crumb rubber, which is confirmed to carry hundreds of chemicals with potentially harmful impacts on health (Zuccaro et al., 2024).

Major pathways contributing to soil emerging as the predominant reservoir of TWPs in the environment include road runoff, atmospheric deposition, and sewage sludge applications (Baensch-Baltruschat et al., 2021; Pang et al., 2023; Wang et al., 2024). Nevertheless, the potential risk posed by the emerging contaminant to terrestrial ecosystems is only in its infancy. After releasing into the soil environment, TWPs can further be subjected to multiple weathered processes, including temperature, humidity, light, shear stress, biofilm colonization, and so on (Hartmann et al., 2019; He et al., 2024; Wagner et al., 2022). Of these, light irradiation is one of the crucial weathered factors triggering the transformation of contaminants, which, in turn, influences their physicochemical properties and environmental behavior. TWPs could be oxidized by light, which can further alter their chemical (adsorption metal ion) and colloidal (dispersion and aggregation) stability, as well as their migration capability (Chen et al., 2024; Ren et al., 2021; Yi et al., 2024). Aged MPs coexisting with other pollutants may cause severer combined environmental issues. So far, there have been many reports about the effect of traditional aged MPs on the carrier capacity, pollutant transport, and co-transport of pollutants in soils, providing a valuable reference for assessing the potential threat posed by the co-existence of MPs and various pollutants in terrestrial ecosystems (An et al., 2023; Chang et al., 2024; Liu et al., 2024a). However, because of the complex components of TWPs, these studies results obtained from traditional MPs are not absolutely applicable to TWPs (Fan et al., 2021).

As published by UN Habitat's 'the World Cities Report 2022', the world urban population has been developing and is expected to rise by an additional 2.2 billion municipal residents by 2050 (UN Habitat, 2022). Anthropogenic activities common to urban regions, such as industry (e.g., mining and electronics manufacturing), agriculture (e.g., fertilizer and irrigation), and transportation (e.g., brake wear and vehicle exhaust), generate a various series of heavy metal loads of physical, chemical, and biological origin, which initially accumulate on municipal surfaces during dry seasons and are rinsed off by rainwater (Li et al., 2024; Ma et al., 2016). Urban rainwater runoff with excessive concentrations of heavy metals has been identified as a prevalent problem globally and could surpass the thresholds advised in guidelines for portable and recreational usage (Pamuru et al., 2022). Heavy metals have been regarded as one of the most threatened contaminants in rainwater runoff due to their nondegradability, bioaccumulation, and toxicity, posing a risk to receiving water environments (Wijeyawardana et al., 2022).It is reported that Lead, zinc and copper are the most common heavy metals in rainwater runoff, and the toxicity of Pb is greater than the others (Lange et al., 2022). On account of rapid industrialization and urbanization, heavy metal contamination in stormwater and soil has become an increasingly severe problem. Meanwhile, a prominent decline in the pH of rain led to more frequent occurrence of acid rainfall, which has also become global pollution (Zhang et al., 2020a). Acid deposition can result in the release and further downward transport of heavy metals in soil through complex physical and chemical processes, creating serious risks to deep soil and groundwater environments (Ouyang et al., 2017; Qi et al., 2022). Therefore, the fact that heavy metal ions, along with acid stormwater, are inevitably transported in soil has been a challenging environmental problem. However, in the study of such problems, since the widespread existence of TWP in soil has not been paid attention to, scientific research is urgently needed to explore the mechanisms of related environmental behaviors.

Thus, our research aimed to examine the adsorption and transport mechanisms of heavy metal (i.e., Pb in this study) in urban soil contaminated by TWP with or without photoaging under acid rain condition with a view to assessing how TWP with environmentally relevant concentrations might affect the retention of Pb in soil. To clarify this issue, batch equilibrium adsorption experiments, 1-D miscible displacement column experiments, and numerical modeling methods are used. The gained results can broaden our comprehension of the environmental behavior at acid rain, Pb, and TWP co-contaminated sites and highlight the remobilization risk assessment of lead in soil polluted by ubiquitous TWP during acid rainfall, as well as provide scientific insights for the potential threat of TWP to urban soil health.

2. Materials and methods

2.1. Materials and reagents

To get close to the realistic scenario, virgin TWPs (V-TWP) were produced by a tire crushing plant (Henan, China) from mixed car tires by cryo-milling and sieving to a size below 180 μm (Masset et al., 2021). V-TWP were soaked in a 5 % HNO_3 solution for 24 h and stirred at regular intervals to eliminate the interference of trace metals or other pollutants. Subsequently, V-TWP were rinsed three times with Milli-Q water, dried in a freeze dryer for 24 h at –50 °C, and sealed away from light in reserve. In order to better explore the variations in the physicochemical characteristics of TWP after natural photoaging, V-TWP in a glass Petri dish were constantly exposed to a mercury lamp with a UVA intensity of 4.50 mW/cm^2 for two weeks (comparable to that of natural sunlight (4.36 mW/cm^2) (Jiang et al., 2023)), flipped every 12 h to ensure uniform illumination. The photoaged TWPs (A-TWP) were saved in the same environment as V-TWP. See Text S1 for information on detailed characterization methods for TWP.

Hunan Province is the representative of the acid rain region in Central China. According to 'the Ecological Environmental State Bulletin of Hunan Province' from 2018 to 2022 (Ecology and Environment Department of Hunan, China, 2018–2022), the annual average pH of precipitation in Hunan Province was 5.18. Considering that the extreme pH of acid rain in 1995 was 3.53 and the pH value of daily monitored precipitation fluctuated, the pH of the simulated acid rain (SAR) was set at 3.5, 4.5, and 5.6 for the purpose of simulating strong acid rain, classic acid rain, and critical acid rain. The SAR stock solution was prepared by mixing 0.5 M H_2SO_4 and 0.5 M HNO_3 at $n(SO_4^{2-}):n(NO_3^-)$ of 4:1, which corresponded to the mean anion compositions of acidic rainwater in Hunan Province (Fei et al., 2020), and SAR work solutions with the desired pH were obtained by diluting the SAR stock solution with Milli-Q water.

Analytical pure-grade chemicals (Hushi, Shanghai, China) and quartz sand with a size of ~ 0.50 mm (Hushi, Shanghai, China) were used for experiments. The pretreatment method for quartz sand and data quality assurance were placed in Text S2.

2.2. Soil collection and incubation

Urban soil utilized was sampled in November 2022 from an area away from roads located in Changsha, Hunan Province, China (28°10′18.7″N, 112°57′16.5″E). Briefly, a shovel was used to take a soil sample at a depth of 0–20 cm from each of the five 5 × 5 m sampling plots that were chosen at the sampling site. Then, all soil samples were manually homogenized, air-dried, and screened through a 10-mesh sieve for further experiments. Referring to a prior investigation to determine the background concentration of TWP (Thomas et al., 2022), the results of extraction procedures showed almost no suspicious black particles in the sampled soil visually.

Taking into account the concentrations of TWP that really existed in the natural soils (Dolar et al., 2021), a series of concentrations, i.e., 0.1 %, 1 %, and 10 % (w/w), were designed. Soils were put into glass beakers covered with water-tight exchange and gas-permeable

membranes and cultured in a dark incubator (25 °C) for 90 days. To ensure that the moisture of 50 % (v/w) was maintained, these beakers were weighed every two days. The control treatment without artificially added V-TWP/A-TWP was also incubated. After incubation, soils were grounded and sieved in a 10-mesh sieve, stored at 4 °C until use. The sampled soil or soil-TWP mixtures were abbreviated to Pure Soil, *S*+0.1 % V-TWP, *S*+0.1 % A-TWP, *S*+1 % V-TWP, *S*+1 % A-TWP, *S*+10 % V-TWP and *S*+10 % A-TWP, respectively. The detail information on soil characterization were described in Text S3.

2.3. Batch adsorption experiments

Adsorption isotherm experiments were carried out in 50 mL centrifuge tubes containing Pb(II) work solutions of different concentrations (60–140 mg/L) under diverse acid rainwater environments, using 5 g/L dosages of sampled soil or soil-TWP mixtures (content of TWP, w/w: 0.1, 1, and 10 %). Pb(II) work solutions (containing 0.01 M $NaNO_3$) were prepared by dissolving $Pb(NO_3)_2$ in three SAR work solutions with various pH of 3.5, 4.5, and 5.6 (adjusting pH using 0.01 M NaOH or HNO_3 if necessary). Subsequently, these tubes were set on the thermostat shaker at 180 rpm for 24 h at 25 °C (enough to reach adsorption equilibrium for every tube). The solutions after equilibrium were centrifuged at 6000 rpm for 10 min and filtered through 0.45 μm filter paper for analysis of the Pb(II) concentrations, which were determined by flame atomic absorption spectrophotometer (PinAAcle900F, USA). Interestingly, preliminary tests indicated a wide distinction in the time to reach adsorption equilibrium between sampled soil and soil-TWP mixtures. Hence, adsorption kinetics experiments were essential, which were conducted in tubes containing 100 mg/L Pb(II) solution at pH = 4.5 on the shaker. The test conditions and absorbents dosages were identical to those used in isotherm tests. A blank treatment without soil and three replicates were included for each experiment.

2.4. Column transport experiments

Transport experiments of Pb(II) were conducted in diverse soil columns at 25 °C with saturated flow conditions. Concretely, acrylic columns of 20.0 cm in length and 2.0 cm in inner diameter were applied for all column tests (Fig. 1). A stainless steel screen (50 μm in pore size) was employed to seal the column bottom, followed by a 10 mm quartz sand layer (exhibiting essentially negligible adsorption to Pb(II) in preliminary experiments) to support the soil particles. Subsequently, a peristaltic pump (Lead Fluid BT600L, China) was used to inject the SAR solution at pH = 4.5 from the column bottom to a predetermined height. After that, the column was packed with air-dried soils in 4–5 mm increments under vibration and progressively saturated with the SAR solution to prevent air entrapment and ensure uniform packing until it reached 40 mm in height. Before the column experiment, the packed column was flushed by the SAR solution for several hours to remove the suspended impurities and balance the hydrodynamic and chemical conditions (negligible leaching of lead). 100 mg/L Pb(II) work solution at pH = 4.5 was pumped to the column for about 96 h and transported from the top down. Constant water head of 100 mm was maintained during the column experiment. And the effluent were routinely collected using a homemade fraction collector (combine timing switches with rotating trays). To characterize the hydraulic conditions of the columns, potassium iodide (KI), following the typical transport pattern, was employed as a conservative tracer. The concentration of I^- was analyzed using Ion Chromatography (Thermo Fisher Scientific ICS-600, USA). Solutes breakthrough curves (BTCs) were plotted based on the normalized effluent concentration (C/C_0) (i.e., the ratio of effluent concentration to influent concentration) versus time. Upon completion of the transport tests, the soil within the column was air-dried and evenly divided into five parts. Later, the Pb concentrations in these sections were determined using the methodology described in HJ 491–2019, China.

2.5. Data analysis and modeling

The adsorption kinetics of Pb(II) onto soils are fitted with the pseudo-first-order and pseudo-second-order kinetic models, while the adsorption isotherms are fitted with the Langmuir and Freundlich models. BTCs of I^- are fitted with the deterministic equilibrium convection-dispersion model (CDM); BTCs of Pb(II) are fitted with the linear or nonlinear two-site sorption model (TSM, a deterministic nonequilibrium CDM). Simulations of measured BTCs concerning transport parameters using CDM are conducted in the Hydrus-1D software (version 4.16). Meanwhile, measured BTCs concerning Pb(II) adsorption parameters in a continuous flow system (i.e., column experiments) are fitted by the Thomas and Yan models. The details for modeling and related equations were documented in Texts S4–S6. Data were plotted using Origin 2024.

3. Results and discussion

3.1. Characterization of aged TWP and tested soils

Comparative analysis results of SEM indicated that the microcosmic surface morphology of TWP with/without photoaging both had granular protrusions presumed to be carbon black particles (Fig. 2a). The V-TWP presented an oligoporous and uneven but relatively smooth surface structure. However, the A-TWP exhibited a polyporous surface where a noticeable variation was observed. The surface of A-TWP showed a more

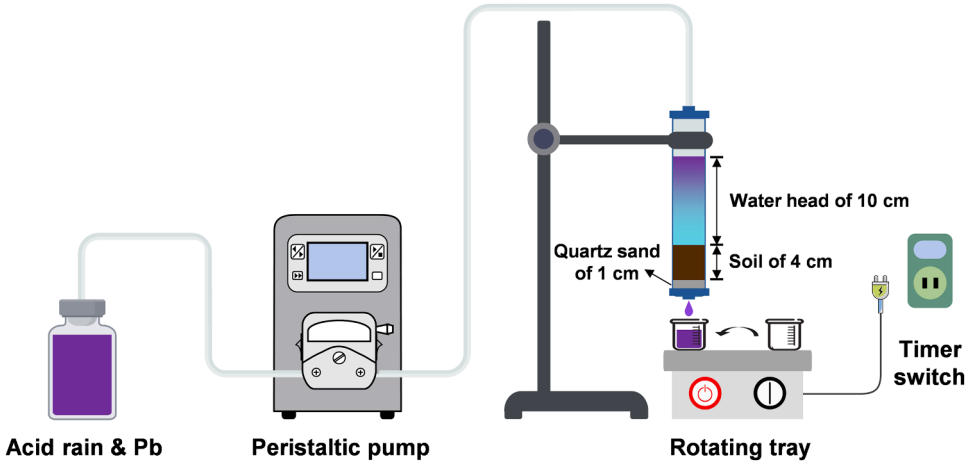

Fig. 1. Diagram of the experimental set-up for column transport.

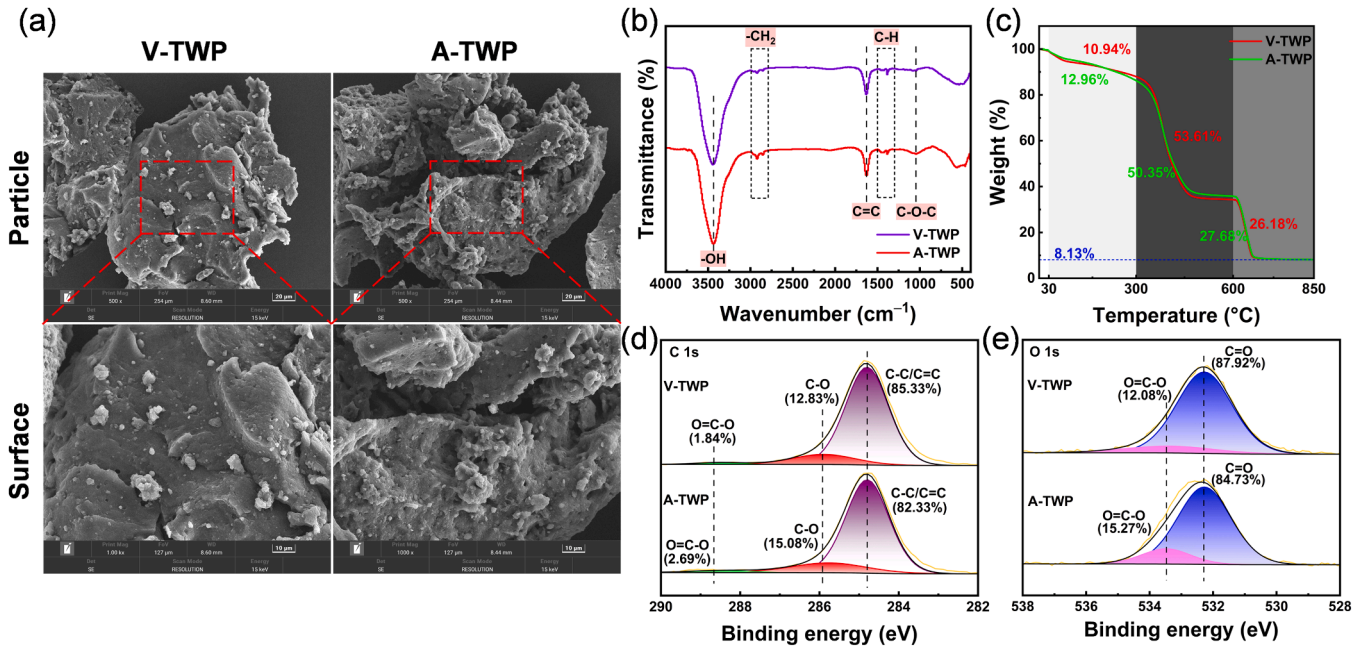

Fig. 2. Characterization of the virgin and photoaged TWP. SEM images (a), FTIR spectra (b), and TGA diagram (c) of the TWP. XPS split-peak fitting for C 1 s (d) and O 1 s (e) in TWP.

pronounced roughness, accompanied by the formation of an evident dendritic protrusion structure. Additionally, the increased specific surface area (from 0.4038 to 0.8633 m^2/g) and the decreased mean particle size (from 155.11 to 140.64 μm) of the A-TWP further demonstrated that the surface of A-TWP was rougher and the pore structure developed more adequately (Table S1). The above information suggested that the photoaging of TWP was longitudinally deep, which was similar to the findings of prior researches (Chen et al., 2024).

As shown in FTIR spectra (Fig. 2b), the intensity of bands in A-TWP was strongly enhanced, including the symmetric stretching vibration of –OH at 3437 cm^{-1}, asymmetric and symmetric stretching vibration of $–CH_2$ at 2920 and 2854 cm^{-1}, and asymmetric stretching vibration of C–O–C at 1043 cm^{-1}. Meanwhile, the intensity of the peaks at 1630 and 1440–1382 cm^{-1}, corresponding to C=C stretching vibration and C–H bending vibration, was decreased, and 700 cm^{-1} fingerprint areas (aromatic/olefin C–H) changed slightly. TGA analysis revealed that the content of volatile substances (30–300 °C) and carbon black (600–850 °C) increased by 2.02 % and 1.50 %, respectively, and the rubber polymeric substances (300–600 °C) in A-TWP were reduced from 53.61 to 50.35 %, suggesting a greater quantity of rubber compositions were decomposed during the photoaging process (Fig. 2c). Based on the results of FTIR and TGA, the aging mechanism was preliminarily speculated. The increase in oxygen-containing functional groups of A-TWP may be primarily attributed to C–H and C=C bonds of rubber long-carbon chains deconstructing and recombining during photoaging. The C–H bond reacted with oxygen to generate peroxy radicals and absorbed hydrogen from the ambient environments, leading to the formation of $–CH_2$ and –OH (Wang et al., 2020). C–H and C=C bonds after rupture absorbed oxygen and generated hydroperoxides, resulting in the generation of C–O–C (Huang et al., 2023). Eventually, free radicals collide each other, generating small-molecule products or further crosslinking to form cyclic aromatic compounds. XPS spectra could evaluate the surface elemental components and chemical states of TWP (Figure S1 and Table S2). In comparison to V-TWP, all the peak areas of O=C–O and C–O determined by C 1 s or those of O=C–O and C=O determined by O 1 s in A-TWP increased (Fig. 2d, 2e and Table S3). The ratio of O/C and the polarity index ($O + N$)/C in A-TWP both increased by 1.97 % and 1.25 %, respectively, supporting that the TWP surface was oxidized under UV irradiation (Duan et al., 2021). Additionally, the A-TWP tended to have more negative charge, and the zeta potential of TWP decreased with increasing pH (Table S4 and Figure S2). In conclusion, the photoaging evidently altered the morphology, size, and surface chemistry of TWP, which have an important effect on their capture performance.

The physicochemical properties of the sampled soil are listed in Table S5. With reference to Wade et al. (2021), total lead content (117 mg kg^{-1}) in the sampled soil is below the average level (220 mg kg^{-1}) in urban soils and ranges from 50 to 200 mg kg^{-1}, indicating that the sampled urban soil was well represented. As Figure S3 and Table S6 presented, although the absorption peaks positions of sampled soil or soil-TWP mixtures were similar, the peaks intensity at the same position was diverse. The characteristic adsorption peaks at 3697 and 3620 cm^{-1} exhibited a slight shifting, which was responsible for the N–H or O–H stretching vibration of inner surfaces of kaolinite (Liu et al., 2023a). Likewise, a slight shifting of the peaks at 1636 and 1032 cm^{-1} was attributed to the C=O stretching of the carboxyl group. The peaks at 796, 693, 534, and 471 cm^{-1}, related to quartz, were unchanged basically. Particularly, the peak at 3438 cm^{-1} (stretching vibration of O–H) exhibited an apparent and regular shifting, and it shifted to 3445 cm^{-1} in S+10% A-TWP. These findings suggested that the incorporation of TWP may introduce more oxygen-containing groups into the sampled soil, enhancing the soils' hydrophilicity and promoting their adsorption of heavy metals. Furthermore, the pronounced changes in other soil properties (e.g., bulk density, soil texture, and zeta potential) will affect the internal channels for transporting solutions (Table S4 and S10, Figure S2 and S4). The physicochemical properties of soils after incubation varied remarkably, which had a crucial influence on the retention of solutes in the soil.

3.2. *Effect of TWP on the adsorption of Pb(II) by soil*

As presented in Fig. 3a, the Pb(II) adsorption amount increased over time. The presence of TWP remarkably enhanced the adsorption of Pb (II) by soil and effectively prolonged the time to reach adsorption equilibrium. This was contrary to the inhibition effect shown by conventional MPs (Liu et al., 2024b), mainly because TWPs, a composite sorbent material, contained a certain proportion of carbon black powder with stronger sorption domains than polymer (i.e., rubber) participating

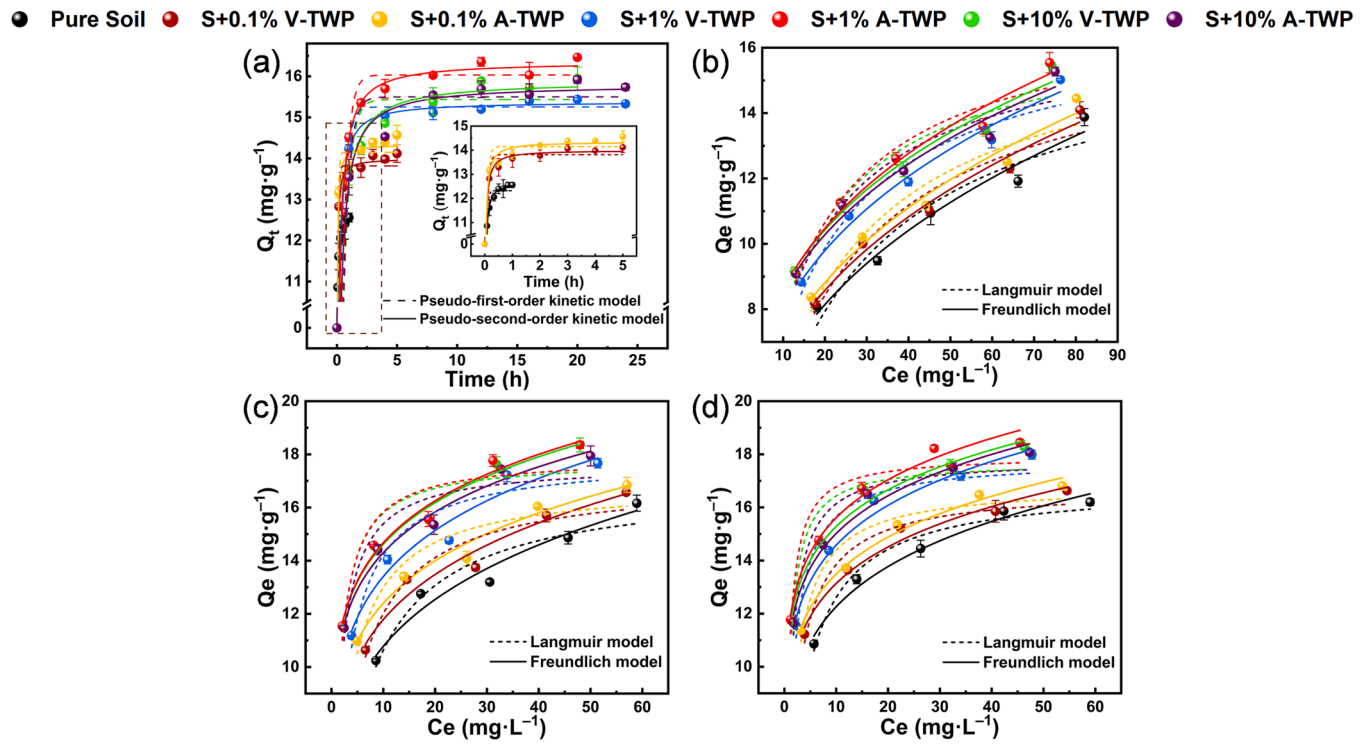

Fig. 3. (a) Adsorption kinetics of 100 mg/L Pb(II) onto soils at pH = 4.5. Adsorption isotherms of 60–140 mg/L Pb(II) onto soils at pH = 3.5 (b), pH = 4.5 (c), and pH = 5.6 (d). Data are presented as the mean ± standard deviation (n = 3).

in adsorption (Sattayanurak et al., 2020). The adsorption equilibrium time of Pure Soil was approximately 1 h, while that of S+0.1% V-TWP/A-TWP was about 4 h, and that of other soils was approximately 12–16 h. It was indicated that Pb(II) may be mainly adsorbed on the surface of soil particles rather than TWPs in the early rapid adsorption stage. Parameters of the Pb(II) adsorption kinetic models are listed in Table S7. It could be observed that the pseudo-second-order kinetic model ($R^2 \geq 0.998$) fits the experimental data on adsorption kinetics more accurately than the pseudo-first-order kinetic model ($R^2 \geq 0.992$), demonstrating that a chemical adsorption involving valence forces generated by sharing or exchanging electrons was the rate-limiting step of the Pb(II) adsorption process (Song et al., 2018).

As illustrated in Fig. 3b–3d and Table S8, the Pb(II) adsorption isotherms are better fitted with the Freundlich model (higher R^2), indicating that Pb(II) adsorption onto soils was a multilayer and heterogeneous adsorption process (Liu et al., 2022a). Meanwhile, the changes in Pb(II) adsorption isotherms under different simulated acid rain environments suggested the Pb(II) adsorption amount by soils decreased with the decrease in pH. This phenomenon may be ascribed to the fact that the soils were more susceptible to protonation at a lower pH, hindering soil chelation with Pb(II) and reducing the stability of soil organic matter-heavy metal complexes. Moreover, the soil's negative electrification was diminished with the decrease in pH (Figure S2), leading to a weakened electrostatic gravitational force between soils and Pb(II). Meanwhile, as shown in Table S9, conventional MPs in general environments (close to neutral or similar to a pH of this study) exhibited a 'dilution effect' on the soil's ability to adsorb heavy metals, which was in contrast to the facilitation effect of TWP, mainly because they would occupy the soil's adsorption sites rather than provide them. Notably, in soils treated with the same concentration of TWP (except for 10 %), the Pb(II) adsorption capacity of A-TWP-treated soils was memorably stronger than that of V-TWP-treated soils (e.g., the value of 1/n in pH = 4.5: S+0.1% V-TWP (0.194) < S+0.1% A-TWP (0.175), S+1% V-TWP (0.176) < S+1% A-TWP (0.148), S+10% A-TWP (0.148) < S+10% V-TWP (0.147)). The evident changes in pore structure, zeta potential, S_{BET}, oxygen-containing functional groups, and major components of TWP after photoaging might be the dominant reasons for the discrepancies in adsorption behaviors between V-TWP-treated soils and A-TWP-treated soils at concentrations of 0.1 % and 1 %. Since the photoaging process would result in the disintegration of coarser TWP into finer ones (consistent with the particle size characterization results), low-density and tiny A-TWP was more prone to suspension and agglomeration than V-TWP (Klöckner et al., 2020), contributing to that A-TWPs separated from soil were apt to adhere to the centrifugal tube wall and were not fully involved in the reaction during oscillation adsorption. The phenomenon inevitably occurred in soil with a higher content of A-TWP, which explained the abnormal adsorption in S+10% A-TWP. Particularly in terms of data fitting trends, V-TWP exhibited a regular accelerative effect of Pb(II) adsorption onto soil (Pure Soil < S+0.1% V-TWP < S+1% V-TWP < S+10% V-TWP), whereas A-TWP showed an irregular boosting effect (Pure Soil < S+0.1% A-TWP < S+10% A-TWP < S+1% A-TWP). Despite the relative content of soil particles was reduced in soil-TWP mixtures, the interaction between TWPs and soil particles could provide more adsorption sites to intensify the Pb(II) adsorption capacity of soils. Moreover, the aging of TWP during soil cultivation may also facilitate the generation of environmentally persistent free radicals (EPFRs), a pervasive kind of free radicals that can stay stable for months and react with water in diverse ways to produce reactive oxygen species (ROS), thereby affecting key adsorption mechanisms (Xu et al., 2023). Simultaneously, the addition of TWP changed the pore structure, chemical functional groups, and bacterial communities in soils, thus changing the adsorption and transport ability to Pb(II) (Liu et al., 2023b, 2024c).

3.3. *Effect of TWP on the transport of Pb(II) in soil*

3.3.1. *Simulations of measured BTCs concerning transport parameters using CDM*

Ground on the assumption that the tracer (I^-) is non-reactive and cannot be adsorbed by soils (retardation factor = 1), use the

deterministic equilibrium CDM model by manually intervening the water content value iteration range (between actual water content and theoretical saturated water content) and its embedded neural network prediction module in Hydrus-1D to estimate hydraulic parameters of the soil columns, such as the dispersivity (d), the saturated hydraulic conductivity (K_s), and the darcy velocity (J_w). The soil bulk weight and texture of each soil column are different, resulting in a certain variability among these parameters. As shown in Fig. 4a and Table S10, the BTCs of I^- in all soil columns were almost symmetrical, and the simulated BTCs of I^- were in good agreement with the measured BTCs ($R^2 \geq 0.983$). The good repeatability of tracer experiments indicated that the experimental methods were feasible to manifest hydrodynamic conditions of the columns, implying that each soil column was filled well and was not impacted by preferential flows or wall effects throughout the experiment. Nevertheless, the equilibrium CDM is unsuitable to model the Pb (II) BTCs (data not shown). The measured BTCs of Pb(II) are fitted by the nonequilibrium TSM, which incorporates a linear or nonlinear sorption assumption based on the Freundlich model.

For soil columns incorporated with 0, 0.1, 1, and 10 % V-TWP, the C/C_0 values of Pb(II) after 96 h were determined as 0.75, 0.68, 0.61, and 0.49, respectively; for soil columns incorporated with 0.1, 1, and 10 % A-TWP, the C/C_0 values were equivalent to 0.64, 0.62, and 0.48, respectively (Fig. 4b and 4c). According to simulation results fitted by linear TSM (Tables S11 and S12), optimized parameters, such as the partitioning coefficient (K_d), the first-order kinetic rate coefficient (α), and the fraction of instantaneous sorption (f), were obtained. Particularly with the increase in V-TWP/A-TWP content, the growth trend of the column-derived K_d values (Pure Soil < *S*+0.1% V-TWP < *S*+0.1% A-TWP < *S*+1% V-TWP < *S*+10% A-TWP < *S*+10% V-TWP < *S*+1% A-TWP) did not always coincide with that of the batch-derived K_F values (Pure Soil < *S*+0.1% V-TWP < *S*+0.1% A-TWP < *S*+1% V-TWP < *S*+1% A-TWP < *S*+10% V-TWP < *S*+10% A-TWP). With the support of various characterization and adsorption results, it seemed that the variation rule of the Pb(II) distribution coefficient obtained by the column tests was more consistent with the real situation. As also reported previously, transfer rules simulated by the TSM were found to be more realistic in heavy metal-polluted agricultural soils (Rheinheimer dos Santos et al., 2013). Similarly, previous studies have also reported obvious inconsistencies in the conclusions drawn between equilibrium adsorption and column tests (Aly et al., 2018; Yang et al., 2022). Experimental constraints (e.g., agitation of samples, soil-water ratios) and analytical imprecision (e.g., errors/variations) may be responsible for these observations (Van Glubt et al., 2021). The values of f and partitioning coefficient (β) diminished gradually with the increase in TWP addition, apart from *S*+0.1% A-TWP, implying that the interaction between TWPs and soil particles could provide more rate-limited sorption sites to enhance the Pb(II) adsorption capacity of soil and prolong breakthrough time. The teeny values of α ($\leq$ 4.1E-07) meant slower Pb(II) nonequilibrium mass transfer rates in these soils contaminated by TWP. Besides, extra proof for the nonequilibrium transfer of Pb(II) in the soil-TWP mixture column was provided by the lower values of the mass migration coefficient ($\omega \leq$ 9.6E-04). The retardation factor (R) increased from 1.098 to 13.90 or to 16.38, respectively, with the increasing content of V-TWP or A-TWP in soil (from 0 % to 10 %), reflecting a reinforced resistance of Pb(II) transport through the soil columns after the incorporation of TWP. It was interpreted as the stronger Pb(II) adsorption affinity of TWP-treated soils. Moreover, the higher R values in the A-TWP-treated soils than the V-TWP-treated soils suggested that a more obvious effect of slowing down in the A-TWP-treated soils. Meanwhile, the inhibitory effect of TWP on the transport of heavy metals in soils was still opposite to the promotional effect of conventional MPs reported in previous studies (Chang et al., 2024; Zhang et al., 2020b). Nevertheless, it does not mean that the larger R is, the longer the breakthrough time is. Especially, 1 % TWP-treated soils showed a longer breakthrough time (approximately 24 h) than other soils (Fig. 4b and 4c), which can be ascribed to the fact that different concentrations of TWP change the pore structure of soils to different degrees. Therefore, 1 % TWP-treated soils with the clearly larger dispersivity (d) had more tortuous pores channels

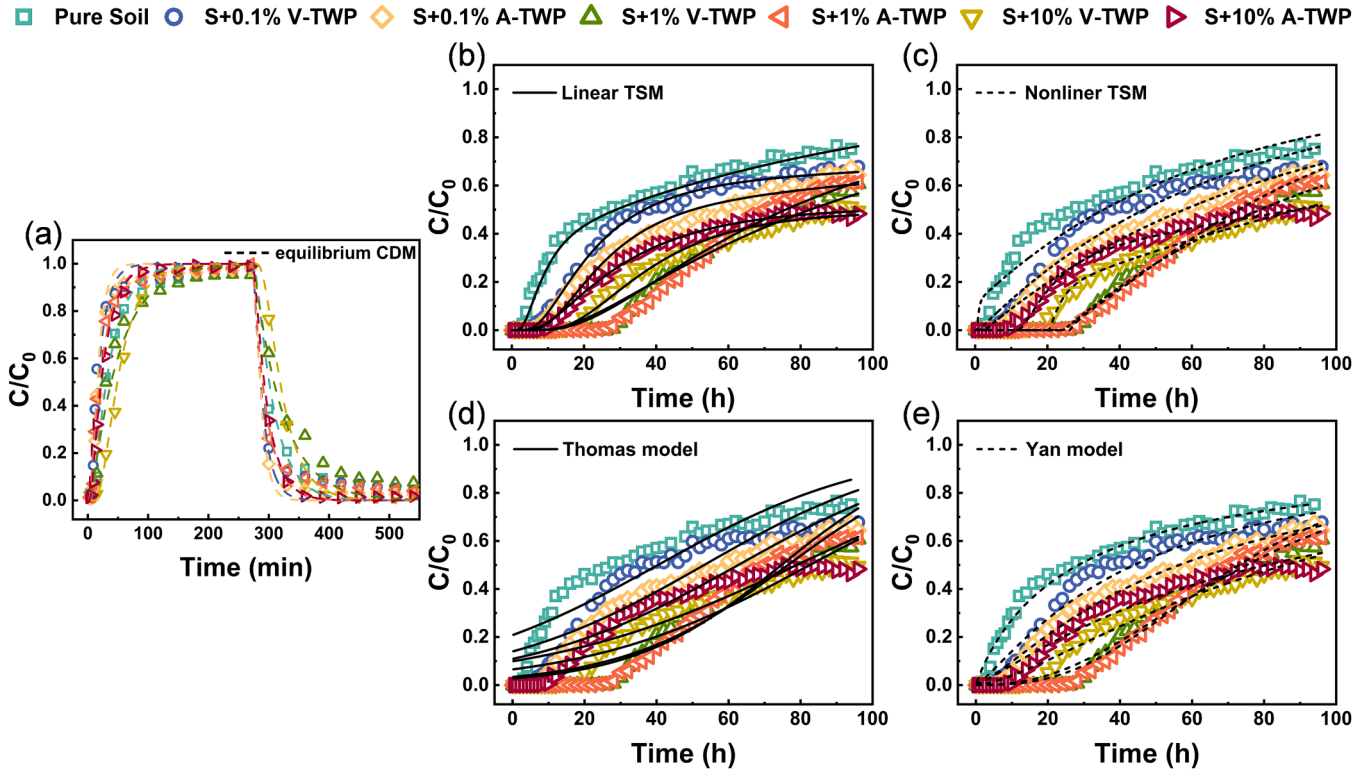

Fig. 4. (a) I^- breakthrough curves fitted by equilibrium CDM. Pb(II) breakthrough curve fitted by linear (b) or nonlinear (c) two-site sorption model (TSM), Thomas model (d), and Yan model (e).

(Table S10), bringing about the slower Pb(II) transport process in the soil column. In addition, the d of V-TWP-treated soils was greater than that of A-TWP-treated soils. Firstly, on account of stronger electrostatic attraction and ligand exchange, A-TWP may exhibit stronger interactions with positively charged iron oxides (e.g., magnetite or goethite) compared to V-TWP. Secondly, due to enhanced ligand exchange between O-containing functional groups with hydroxyl groups on mineral surfaces, the A-TWP adsorption on negatively charged clay minerals (e.g., montmorillonite or kaolinite) may be intensified (Xu et al., 2024). Consequently, we speculated that the stronger interactions between A-TWP and minerals make A-TWP more vulnerable to heteroaggregation, adsorption, and co-precipitation with minerals, influencing the distribution of soil pore throat.

Comparative results of the output parameter simulated by linear TSM and nonlinear TSM suggested that the changing trend of column-derived K_d values showed excellent agreement between them, while that of f values was just the opposite (Tables S11 and S12). Analogously, the variation tendency of 1/n values fitted by nonlinear TSM was also not consistent with 1/n values obtained from the Freundlich model. Although the data of BTCs were well fitted by linear TSM or nonlinear TSM, giving relatively high correlation coefficients ($R^2 \geq 0.984$ or 0.951), the model with the lower values of Akaike Information Criterion (AIC) and Bayesian Information Criterion (BIC) would be chosen by advantage. Accordingly, the simulation incorporating the nonlinear sorption assumption strengthened the model goodness in soils with a higher proportion of TWP (1, 10 %) compared to the linear sorption assumption but reduced the model goodness in soils with a lower proportion of TWP (0, 0.1 %), revealing more critical effects of sorption nonlinearity on the retention of Pb(II) in the presence of 1 or 10 % TWP under the experimental conditions. In summary, it is an indication of the complexity of Pb(II) sorption mechanisms in TWP-treated soils, and nonlinear sorption replaced linear sorption as the main Pb(II) sorption mechanism in soils with a higher concentration of TWP (1, 10 %). Given that the f simulated by nonlinear TSM increased bit by bit with the growth in TWP addition, the instantaneous sorption/desorption equilibrium sites of Pb(II) in soils increased gradually, hinting that more Pb (II) could be rapidly transferred from the soils to the water phase, possibly during recurrent rainfall and other waterlogging events. Noteworthy, no matter linear TSM or nonlinear TSM, the fitted f value in A-TWP-treated soils was larger than that in V-TWP-treated soils. Therefore, the incorporation of higher concentrations of photoaged TWP may enhance the Pb(II) potential risks of mobilization into deeper soil and groundwater environments. Furthermore, according to the Pb(II) adsorption isotherms under different acid rainwater environments, the more severe environmental risks of Pb(II) to terrestrial ecosystems with the change in pH from various perspectives can be predicted. Briefly, enhanced Pb(II) sorption capacity of soils at a higher pH (pH = 5.6) would lead to more Pb(II) accumulation in the topsoil environments; acidic stormwater co-existing with unadsorbed Pb(II) at a lower pH (pH = 3.5) would transport into deeper soil and groundwater environments.

3.3.2. *Simulations of measured BTCs concerning adsorption parameters using Thomas and Yan models*

As shown in Fig. 4d, 4e and Table S13, the Yan model was better at fitting the BTCs ($R^2 \geq 0.963$) compared to the Thomas model. The boosting trend of q_T (all soils apart from 10 % TWP-treated soils) or q_Y (all soils apart from 1 % TWP-treated soils) was in line with that of column-derived K_d values, further confirming the above conclusion (the Pb(II) partitioning trend reflected in column tests was more realistic). The observed abnormity of q_T and q_Y may be attributed to the Thomas and Yan models exclusively focuses on adsorption and does not take soil characteristics such as pore dispersion into account. In addition, as a consequence of a shorter retention period in column experiments, the maximum adsorption capacity values (q_T and q_Y) obtained from the Thomas and Yan models were all below those (K_L) derived from batch experiments (Table S8). The smaller values of rate constants, which describe the transfer rate of Pb(II) from the liquid to the soil, indicated a higher decline in the adsorption rate with increasing time as a result of fewer unoccupied adsorption sites. The rate constants (K_Y) in A-TWP-treated soils were markedly lower than those in V-TWP-treated soils, which suggested that the BTCs of A-TWP-treated soils tended to flatten out more quickly. In addition, the BTCs of 1 % TWP-treated soils with the maximum K_Y were the steepest, while the BTCs of Pure Soil with the minimum K_Y was the flattest. In short, the Thomas and Yan models could help analyse the results of the BTCs better.

3.3.3. *Retention of Pb(II) in soil*

Although the retention profile at 96 h did not accurately reflect the lead vertical distribution situation when Pb(II) completely penetrated the soil bottom, the lead vertical distribution trend in soil columns contaminated with the same concentrations of V-TWP or A-TWP exhibited a similar pattern at the moment (Fig. 5). The lead concentration of each layer in Pure Soil showed minimal variation, whereas those in other soils displayed significant disparities. The notable effect of TWP on the retention behavior of Pb(II) may be ascribed to the fact that TWP affected the physicochemical reactions (e.g., mechanical resistance, sorption, and chelation) involved in the Pb(II) transport by altering the physicochemical properties of the soil. Besides, from left to right in Fig. 5, the lead concentrations in the upper sections were 10.6, 11.53, 11.33, 15.6, 11.99, 12.7, and 16.4 mg g^{-1}, whereas those in the bottom sections were 10.6, 11.56, 12.03, 4.29, 11.75, 13.86, and 2.62 mg g^{-1}, respectively. It can be inferred that TWP observably facilitated lead accumulation on the topsoil and impeded lead transport into the deeper soil layer. Moreover, TWP effectively enhanced the soil's ability to adsorb lead and extended the time required for adsorption equilibrium, which entirely aligned with the above conclusions of batch adsorption experiments.

4. Conclusions and environmental implications

This study employed experimental and numerical methods to initially elucidate the adsorption and transport mechanisms of Pb(II) in urban soils contaminated by ubiquitously photoaged TWP under acid rainfall. Specifically, TWP dramatically enhanced the adsorption capacity and retardation factor of Pb(II) in soils, which led to the Pb(II) initial accumulation in the topsoils and the Pb(II) hindered downward transport, thereby intensifying the Pb(II) retention risks in surface soil environments. And the promotion effect of photoaged TWP was more

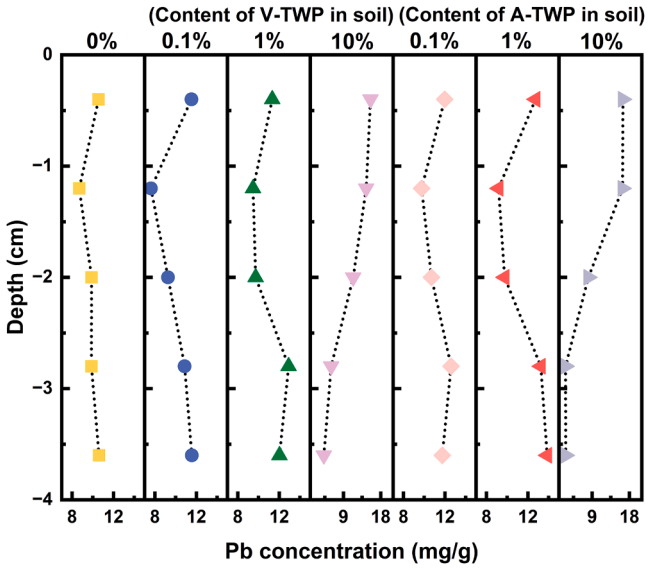

Fig. 5. Retention profiles of Pb in soil column.

pronounced than virgin TWP. Based on the simulated results by TSM, higher concentrations of photoaged TWP will enhance the Pb(II) potential risks of downward mobilization into deeper soil and groundwater environments if multiple rainfalls or other waterlogging events occur. Besides, this study emphasized the key role of nonlinear sorption in the retention of Pb(II) in the presence of 1 or 10 % TWP and underscored the implications of TWP on the Pb(II) harmful environmental risks in soil under different acid rain environments according to results of batch and column experiments. Given that soil organisms are inevitably exposed to TWP and Pb(II), more attention is warranted to the terrestrial ecological impact of TWP under environmentally relevant exposure conditions. Additionally, it should be noted that future work is strongly recommended to investigate the relative role of other factors (e.g., composite aging of TWP, the cotransport of TWPs themselves or leachates, more complicated rainfall, field scales) on the Pb(II) migration behaviors in urban soils to narrow the gaps between the laboratory and natural environments. In total, this research provides crucial insights into the effects of TWP on the geochemistry process and severer potential environmental risks of Pb(II) in urban soils, which will contribute to calling attention to the correct disposal and recycling of spent tire particles or their products.

CRediT authorship contribution statement

Enjie Li: Writing – original draft, Validation, Software, Methodology, Investigation, Data curation. **Jinhui Huang:** Writing – original draft, Supervision, Funding acquisition. **Hanbo Yu:** Validation, Project administration, Conceptualization. **Si Liu:** Resources, Formal analysis. **Wenjuan He:** Investigation. **Wei Zhang:** Software. **Haoliang Pang:** Data curation. **Chenyu Zhang:** Visualization.

Declaration of competing interest

The authors declare that they have no known competing financial interests or personal relationships that could have appeared to influence the work reported in this paper.

Data availability

Data will be made available on request.

Acknowledgments

This study was supported by the Water Conservancy Science and Technology Project of Hunan Province (XSKJ 2022068–20).

Supplementary materials

Supplementary material associated with this article can be found, in the online version, at doi:10.1016/j.watres.2024.122410.

References

Aly, Y.H., Liu, C., McInnis, D.P., Lyon, B.A., Hatton, J., McCarty, M., Arnold, W.A., Pennell, K.D., Simcik, M.F., 2018. Situ remediation method for enhanced sorption of perfluoro-alkyl substances onto ottawa sand. J. Environ. Manage. 144 (9), 04018086.

An, Q.Y., Zhou, T., Wen, C., Yan, C.Z., 2023. The effects of microplastics on heavy metals bioavailability in soils: a meta-analysis. J. Hazard. Mater. 460, 132369.

Baensch-Baltruschat, B., Kocher, B., Kochleus, C., Stock, F., Reifferscheid, G., 2021. Tyre and road wear particles - A calculation of generation, transport and release to water and soil with special regard to German roads. Sci. Total Environ. 752, 141939.

Castan, S., Sherman, A., Peng, R., Zumstein, M.T., Wanek, W., Hüffer, T., Hofmann, T., 2022. Uptake, metabolism, and accumulation of tire wear particle-derived compounds in lettuce. Environ. Sci. Technol. 57 (1), 168–178.

Chang, B.K., Huang, Z.X., Yang, X.D., Yang, T.H., Fang, X.H., Zhong, X.B., Ding, W., Cao, G., Yang, Y.J., Hu, F.A., Xu, C.Y., Qiu, L., Lv, J.L., Du, W., 2024. Adsorption of Pb(II) by UV-aged microplastics and cotransport in homogeneous and heterogeneous porous media. J. Hazard. Mater. 465, 133413.

Chen, L., Liu, Z., Yang, T.H., Zhao, W.J., Yao, Y.Z., Liu, P., Jia, H.Z., 2024. Photoaged tire wear particles leading to the oxidative damage on earthworms (Eisenia fetida) by disrupting the antioxidant defense system: the definitive role of environmental free radicals. Environ. Sci. Technol. 58 (10), 4500–4509.

Dolar, A., Selonen, S., van Gestel, C.A.M., Perc, V., Drobne, D., Jemec Kokalj, A., 2021. Microplastics, chlorpyrifos and their mixtures modulate immune processes in the terrestrial crustacean Porcellio scaber. Sci. Total Environ. 772, 144900.

Duan, J.J., Bolan, N., Li, Y., Ding, S.Y., Atugoda, T., Vithanage, M., Sarkar, B., Tsang, D. C.W., Kirkham, M.B., 2021. Weathering of microplastics and interaction with other coexisting constituents in terrestrial and aquatic environments. Water Res. 196, 117011.

Ecology and Environment Department of Hunan, China, 2018–2022. Ecological Environmental State Bulletin of Hunan Province. http://sthjt.hunan.gov.cn/.

Fan, X., Gan, R., Liu, J., Xie, Y., Xu, D., Xiang, Y., Su, J., Teng, Z., Hou, J., 2021. Adsorption and desorption behaviors of antibiotics by tire wear particles and polyethylene microplastics with or without aging processes. Sci. Total Environ. 771, 145451.

Fei, J.C., Ma, J.J., Yang, J.Q., Liang, Y.J., Ke, Y., Yao, L.W., Li, Y.C., Liu, D.G., Min, X.B., 2020. Effect of simulated acid rain on stability of arsenic calcium residue in residue field. Environ. Geochem. Hlth. 42 (3), 769–780.

Hartmann, N.B., Hüffer, T., Thompson, R.C., Hassellöv, M., Verschoor, A., Daugaard, A. E., Rist, S., Karlsson, T., Brennholt, N., Cole, M., Herrling, M.P., Hess, M.C., Ivleva, N. P., Lusher, A.L., Wagner, M., 2019. Are we speaking the same language? Recommendations for a definition and categorization framework for plastic debris. Environ. Sci. Technol. 53 (3), 1039–1047.

He, W.J., Huang, J.H., Liu, S., Yu, H.B., Li, E.J., Zhang, W., Yi, K.X., Zhang, C.Y., Pang, H. L., Tan, X.F., 2024. Effects of microplastics on sedimentary geochemical properties and microbial ecosystems combined with hydraulic disturbance. Sci. Total Environ. 923, 171350.

He, W.J., Liu, S., Zhang, W., Yi, K.X., Zhang, C.Y., Pang, H.L., Huang, D.L., Huang, J.H., Li, X., 2023. Recent advances on microplastic aging: identification, mechanism, influence factors, and additives release. Sci. Total Environ. 889, 164035.

Huang, W., Deng, J., Liang, J., Xia, X., 2023. Comparison of lead adsorption on the aged conventional microplastics, biodegradable microplastics and environmentally-relevant tire wear particles. Chem. Eng. J. 460, 141838.

Jiang, W., Zhu, K., Ma, H., Liu, J., Zhang, C., Dai, Y., Jia, H., 2023. Sulfur-containing persistent free radicals and reactive species on photoaged microplastics: identification and the formation mechanism. Environ. Sci. Technol. 57 (23), 8680–8690.

Klöckner, P., Seiwert, B., Eisentraut, P., Braun, U., Reemtsma, T., Wagner, S., 2020. Characterization of tire and road wear particles from road runoff indicates highly dynamic particle properties. Water Res. 185, 116262.

Kole, P.J., Löhr, A.J., Van Belleghem, F.G.A.J., Ragas, A.M.J., 2017. Wear and tear of tyres: a stealthy source of microplastics in the environment. Int. J. Environ. Res. Public Health 14, 1265.

Lange, K., Viklander, M., Blecken, G.T., 2022. Investigation of intra-event variations of total, dissolved and truly dissolved metal concentrations in highway runoff and a gross pollutant trap - bioretention stormwater treatment train. Water Res. 216, 118284.

Li, J., Zhang, L.L., Yu, S., Hong, B., Lin, R.H., Li, Q., Jia, H.F., Yang, D.W., Gu, C.W., Jia, Q.M., 2024. Source-sink relationships of anthropogenic metal(loid)s from urban catchment to waterway in relation to spatial pattern of urban green infrastructures. J. Hazard. Mater. 471, 134381.

Liu, J., Li, Y.R., Wang, Y.H., Wang, Y.N., Xu, J.M., Liu, X.M., 2023a. Competitive adsorption of lead and cadmium on soil aggregate at micro-interfaces: multi-surface modeling and spectroscopic studies. J. Hazard. Mater. 448, 130915.

Liu, S., Huang, J.H., He, W.J., Shi, L.X., Zhang, W., Li, E.J., Hu, J.Y., Zhang, C.Y., Pang, H.L., 2024a. Effects of microplastics on microbial community structure and wheatgrass traits in Pb-contaminated riparian sediments under flood-drainage-planting conditions. J. Hazard. Mater. 470, 134283.

Liu, S., Huang, J.H., He, W.J., Shi, L.X., Zhang, W., Li, E.J., Zhang, C.Y., Pang, H.L., 2024b. Impact of polyamide microplastics on riparian sediment structures and Cd (II) adsorption: a comparison of natural exposure, dry-wet cycles, and freeze-thaw cycles. J. Hazard. Mater. 466, 133589.

Liu, S., Huang, J.H., He, W.J., Zhang, W., Yi, K.X., Zhang, C.Y., Pang, H.L., Huang, D.L., Zha, J., Ye, C., 2023b. Impact of microplastics on lead-contaminated riverine sediments: based on the enzyme activities, DOM fractions, and bacterial community structure. J. Hazard. Mater. 447, 130763.

Liu, S., Huang, J.H., Zhang, W., Shi, L.X., Yi, K.X., Zhang, C.Y., Pang, H.L., Li, J.N., Li, S. Z., 2022a. Investigation of the adsorption behavior of Pb(II) onto natural-aged microplastics as affected by salt ions. J. Hazard. Mater. 431, 128643.

Liu, Z., Sun, Y.J., Wang, J.Q., Li, J.H., Jia, H.Z., 2022b. In vitro assessment reveals the effects of environmentally persistent free radicals on the toxicity of photoaged tire wear particles. Environ. Sci. Technol. 56 (3), 1664–1674.

Liu, Z.X., Pang, H.L., Yi, K.X., Wang, X., Zhang, W., Zhang, C.Y., Liu, S., Gu, Y.L., Huang, J.H., Shi, L.X., 2024c. Isolation and application of Bacillus thuringiensis LZX01: efficient membrane biofouling mitigation function and anti-toxicity potential. Bioresour. Technol. 394, 130272.

Luo, H.W., Zeng, Y.F., Zhao, Y.Y., Xiang, Y.H., Li, Y., Pan, X.L., 2021. Effects of advanced oxidation processes on leachates and properties of microplastics. J. Hazard. Mater. 413, 125342.

Ma, Y.K., Egodawatta, P., McGree, J., Liu, A., Goonetilleke, A., 2016. Human health risk assessment of heavy metals in urban stormwater. Sci. Total Environ. 557-558, 764–772.

Masset, T., Ferrari, B.J.D., Oldham, D., Dudefoi, W., Minghetti, M., Schirmer, K., Bergmann, A., Vermeirssen, E., Breider, F., 2021. In vitro digestion of tire particles in a fish model (Oncorhynchus mykiss): solubilization kinetics of heavy metals and effects of food coingestion. Environ. Sci. Technol. 55 (23), 15788–15796.

McIntyre, J.K., Prat, J., Cameron, J., Wetzel, J., Mudrock, E., Peter, K.T., Tian, Z.Y., Mackenzie, C., Lundin, J., Stark, J.D., King, K., Davis, J.W., Kolodziej, E.P., Scholz, N.L., 2021. Treading water: tire wear particle leachate recreates an urban runoff mortality syndrome in coho but not chum salmon. Environ. Sci. Technol. 55 (17), 11767–11774.

Ouyang, W., Huang, W., Hao, X., Tysklind, M., Haglund, P., Hao, F., 2017. Watershed soil Cd loss after long-term agricultural practice and biochar amendment under four rainfall levels. Water Res. 122, 692–700.

Pamuru, S.T., Forgione, E., Croft, K., Kjellerup, B.V., Davis, A.P., 2022. Chemical characterization of urban stormwater: traditional and emerging contaminants. Sci. Total Environ. 813, 151887.

Pang, H.L., Huang, J.H., Li, X., Yi, K.X., Li, S.Z., Liu, Z.X., Zhang, W., Zhang, C.Y., Liu, S., Gu, Y.L., 2023. Enhancing quorum quenching media with 3D robust electrospinning coating: a novel biofouling control strategy for membrane bioreactors. Water Res. 234, 119830.

Qi, S.Q., Li, X.X., Luo, J., Han, R.F., Chen, Q.Q., Shen, D.S., Shentu, J., 2022. Soil heterogeneity influence on the distribution of heavy metals in soil during acid rain infiltration: experimental and numerical modeling. J. Environ. Manage. 322, 116144.

Ren, Z., Gui, X., Wei, Y., Chen, X., Xu, X., Zhao, L., Qiu, H., Cao, X., 2021. Chemical and photo-initiated aging enhances transport risk of microplastics in saturated soils: key factors, mechanisms, and modeling. Water Res. 202.

Rheinheimer dos Santos, D., Cambier, P., Mallmann, F.J., Labanowski, J., Lamy, I., Tessier, D., van Oort, F., 2013. Prospective modeling with Hydrus-2D of 50 years Zn and Pb movements in low and moderately metal-contaminated agricultural soils. J. Contam. Hydrol. 145, 54–66.

Sattayanurak, S., Sahakaro, K., Kaewsakul, W., Dierkes, W.K., Reuvekamp, L.A.E.M., Blume, A., Noordermeer, J.W.M., 2020. Synergistic effect by high specific surface area carbon black as secondary filler in silica reinforced natural rubber tire tread compounds. Polym. Test. 81, 106173.

Song, B., Xu, P., Zeng, G., Gong, J., Wang, X., Yan, J., Wang, S., Zhang, P., Cao, W., Ye, S., 2018. Modeling the transport of sodium dodecyl benzene sulfonate in riverine sediment in the presence of multi-walled carbon nanotubes. Water Res. 129, 20–28.

Sun, T., Cai, S., Zhang, X., Wang, D., Zhang, W., 2024. Leaching hazards of tire wear particles in hydrothermal treatment of sludge: exploring molecular composition, transformation mechanism, and ecological effects of tire wear particle-derived compounds. Water Res. 257, 121669.

Thomas, J., Moosavian, S.K., Cutright, T., Pugh, C., Soucek, M.D., 2022. Method development for separation and analysis of tire and road wear particles from roadside soil samples. Environ. Sci. Technol. 56 (17), 11910–11921.

UN Habitat, 2022. World Cities Report 2022. https://unhabitat.org/wcr/.

Van Glubt, S., Brusseau, M.L., Yan, N., Huang, D.D., Khan, N., Carroll, K.C., 2021. Column versus batch methods for measuring PFOS and PFOA sorption to geomedia. Environ. Pollut. 268, 115917.

Wade, A.M., Richter, D.D., Craft, C.B., Bao, N.Y., Heine, P.R., Osteen, M.C., Tan, K.G., 2021. Urban-soil pedogenesis drives contrasting legacies of lead from paint and gasoline in city soil. Environ. Sci. Technol. 55 (12), 7981–7989.

Wagner, S., Hüffer, T., Klöckner, P., Wehrhahn, M., Hofmann, T., Reemtsma, T., 2018. Tire wear particles in the aquatic environment - A review on generation, analysis, occurrence, fate and effects. Water Res. 139, 83–100.

Wagner, S., Klöckner, P., Reemtsma, T., 2022. Aging of tire and road wear particles in terrestrial and freshwater environments - A review on processes, testing, analysis and impact. Chemosphere 288, 132467.

Wang, C., Xian, Z.Y., Jin, X., Liang, S.J., Chen, Z.H., Pan, B., Wu, B., Ok, Y.S., Gu, C., 2020. Photo-aging of polyvinyl chloride microplastic in the presence of natural organic acids. Water Res. 183, 116082.

Wang, X., Yi, K.X., Pang, H.L., Liu, Z.X., Li, X., Zhang, W., Zhang, C.Y., Liu, S., Huang, J. H., Zhang, C., 2024. An overview of quorum sensing in shaping activated sludge forms: mechanisms, applications and challenges. Sci. Total Environ. 927, 171886.

Wen, J., Sun, H., Yang, B.W., Song, E.R., Song, Y., Jiang, G.B., 2024. Environmentally relevant concentrations of microplastic exposure cause cholestasis and bile acid metabolism dysregulation through a gut-liver loop in mice. Environ. Sci. Technol. 58 (4), 1832–1841.

Wijeyawardana, P., Nanayakkara, N., Gunasekara, C., Karunarathna, A., Law, D., Pramanik, B.K., 2022. Improvement of heavy metal removal from urban runoff using modified pervious concrete. Sci. Total Environ. 815, 152936.

Winkler, A., Santo, N., Ortenzi, M.A., Bolzoni, E., Bacchetta, R., Tremolada, P., 2019. Does mechanical stress cause microplastic release from plastic water bottles? Water Res. 166, 115082.

Xu, Q., Li, G., Fang, L., Sun, Q., Han, R.X., Zhu, Z., Zhu, Y.G., 2023. Enhanced formation of 6PPD-Q during the aging of tire wear particles in anaerobic flooded soils: the role of iron reduction and environmentally persistent free radicals. Environ. Sci. Technol. 57 (14), 5978–5987.

Xu, Y., Ou, Q., van der Hoek, J.P., Liu, G., Lompe, K.M., 2024. Photo-oxidation of micro- and nanoplastics: physical, chemical, and biological effects in environments. Environ. Sci. Technol. 58 (2), 991–1009.

Yang, B., Qiu, H., Zhang, P., He, E., Xia, B., Liu, Y., Zhao, L., Xu, X., Cao, X., 2022. Modeling and visualizing the transport and retention of cationic and oxyanionic metals (Cd and Cr) in saturated soil under various hydrochemical and hydrodynamic conditions. Sci. Total Environ. 812, 151467.

Yi, K.X., Huang, J.H., Pang, H.L., Li, S.Z., Liu, Z.X., Wang, X., Zhang, W., Zhang, C.Y., Liu, S., Gu, Y.L., 2024. Semi-interpenetrating network hydrogels-based microcapsule for quorum quenching bacteria biocontainment to enhance biofouling control in membrane bioreactor. Chem. Eng. J. 486, 150103.

Zhang, C., Yi, X., Gao, X., Wang, M., Shao, C., Lv, Z., Chen, J., Liu, Z., Shen, C., 2020a. Physiological and biochemical responses of tea seedlings (Camellia sinensis) to simulated acid rain conditions. Ecotoxicol. Environ. Saf. 192.

Zhang, S., Han, B., Sun, Y., Wang, F., 2020b. Microplastics influence the adsorption and desorption characteristics of Cd in an agricultural soil. J. Hazard. Mater. 388, 121775.

Zuccaro, P., Thompson, D.C., de Boer, J., Llompart, M., Watterson, A., Bilott, R., Birnbaum, L.S., Vasiliou, V., 2024. The european union ban on microplastics includes artificial turf crumb rubber infill: other nations should follow suit. Environ. Sci. Technol. 58 (6), 2591–2594.